that the SHB effect of the RIM−DFB laser is much smaller than that of the QWS−DFB laser.

IV. SUMMARY

In conclusion, we have proposed a new structure for reducing the spatial hole-burning effect by introducing a different refractive index in the center region of the upper cladding layer. This structure has two effects. One is the distributed effective phase shift effect that reduces the SHB effect, and the other is the distributed coupling coefficient effect that enhances the single-mode gain difference. We have calculated the above-threshold characteristics of the proposed structure, and have compared them with those of other structures. The normalized single-mode gain difference of the RIM−DFB laser is larger than that of the CPM−DFB laser over the whole range of injection current due to a distributed coupling coefficient effect. The variation of the lasing wavelength of the RIM−DFB laser as a function of injection current is small compared to that of the QWS−DFB and the CPM−DFB laser. The length of the center region that enables large normalized single-mode gain difference at a high injection current is calculated to be 0.2−0.4 of the total cavity length.

REFERENCES

1. H. Soda, Y. Kotaki, H. Sudo, H. Ishikawa, S. Yamakoshi, and H. Imai, Stability in single longitudinal mode operation in GaInAsP/InP phase-adjusted DFB lasers, IEEE J Quantum Electron QE-23 (1987), 804−814.
2. G.P. Agrawal, J.E. Geusic, and P.J. Anthony, Distributed feedback lasers with multiple phase-shift regions, Appl Phys Lett 53 (1988), 178−179.
3. M. Okai, N. Chinone, H. Taira, and T. Harada, Corrugation pitch modulated phase-shifted DFB laser, IEEE Photon Technol Lett 1 (1989), 200−201.
4. K. Tada, Y. Nakano, and A. Ushirokawa, Proposal of a distributed feedback laser with nonuniform stripe width for complete single-mode oscillation, Electron Lett 20 (1984), 82−84.
5. B.S.K. Lo and H. Ghafouri-Shiraz, Spectral characteristics of distributed feedback laser diodes with distributed coupling coefficient, J Lightwave Technol 13 (1995), 200−212.
6. T. Fessant and X. Doyelle, Enhanced single-mode operation in multisection DFB lasers with both localized and distributed phase shift, IEEE Photon Technol Lett 10 (1998), 33−35.
7. K.T. Chan, Y.W. Hui, D.J. Han, and G.H. Li, Modification of refractive index of GaAs by ion implantation of oxygen, Nucl Instrum Methods B 83 (1993), 177−180.
8. S.-C. Cho, B.-G. Kim, and N. Dagili, Extended additional layer method of calculating the coupling coefficient of arbitrary shaped gratings, Microwave Opt Technol Lett 16 (1997), 143−145.
9. M. Okai, Spectral characteristics of distributed feedback semiconductor lasers and their improvements by corrugation-pitch-modulated structure, J Appl Phys 75 (1994), 1−29.
10. P. Correc, Stability of phase-shifted DFB lasers against hole burning, IEEE J Quantum Electron 30 (1994), 2467−2476.

A CONFORMAL SPHERICAL – CIRCULAR MICROSTRIP ANTENNA: AXISYMMETRIC EXCITATION BY AN ELECTRIC DIPOLE

Valery V. Radchenko,[1,2] **Alexander I. Nosich,**[1,2] **Jean-Pierre Daniel,**[2] **and Sergey S. Vinogradov**[3]
[1] Institute of Radiophysics and Electronics
National Academy of Sciences
Kharkov 310085, Ukraine
[2] Laboratoire Antennes et Reseaux
Universite de Rennes 1
Rennes 35042, France
[3] Department of Mathematical Sciences
University of Dundee
Dundee DD1 4HN, Scotland

ABSTRACT: *A mathematically accurate method of analysis of a spherical-disk antenna conformally printed on a dielectric-covered metallic sphere is presented. The antenna is fed by a radial coaxial probe simulated by an electric dipole. The solution consists of reducing the boundary-value problem to the dual-series equations, and further to a regularized infinite-matrix equation. This procedure is based on the analytical inversion of the static part of the problem of a disk in free space, and results in a stable and fast algorithm with a guaranteed convergence. Numerical data on the basic antenna characteristics are presented. © 2000 John Wiley & Sons, Inc. Microwave Opt Technol Lett 26: 176−182, 2000.*

1. INTRODUCTION

Metallic circular disks printed on dielectric substrates are used frequently in patch antenna technology. Conformal printed antennas are necessary in automotive and airborne communications and radar due to their low profile and light weight. In this paper, the problem of modeling of a spherical-disk conformal printed antenna is considered assuming an excitation by a coaxial probe. The probe is modeled by a radial electric dipole (RED) located at the surface of the metal sphere covered with dielectric. From a theoretical point of view, such a geometry is a canonical one for a wide class of conformal patch antennas. Previously, similar problems have been analyzed by direct applications of the method of moments [1, 2]. However, convergence of these numerical approximations is not uniformly guaranteed, especially if narrow resonances are present [3]. Patch antennas are essentially resonant devices; hence, this must be kept in mind when developing an accurate simulation software. We propose an exact mathematical method based on the analytical inversion of the free-space static problem for a spherical disk [4, 5] that has been used previously in the analysis of cavity-backed apertures and reflector antennas [6−8]. This method belongs to the broad family of techniques collectively called the method of analytical regularization [9] that are remarkable for stable and fast numerical solutions.

2. PROBLEM FORMULATION

Consider a zero-thickness perfectly electric conducting (PEC) spherical disk of curvature radius c and angular width $2\theta_0$, located on a dielectric substrate of thickness h and dielectric constant ϵ (see Fig. 1). The substrate has a spherical-layer
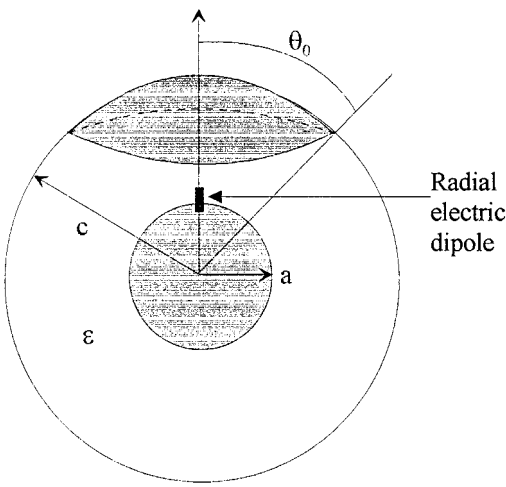
Figure 1 Geometry of the problem

shape, and is backed by a PEC sphere of radius a. The disk is symmetrically excited by a RED located in the substrate at the surface of the metal sphere. The problem is considered in the spherical coordinate system (r, θ, ϕ) having its origin in the center of the sphere. The time dependence is assumed to be $e^{-i\omega t}$.

In the uniform space filled with a dielectric of permittivity ϵ, the field of a RED shifted by a distance a from the origin along the polar axis is known to be

$$E_r^{(0)} = \left(\frac{\partial^2}{\partial r^2} + k_\epsilon^2 \right)(rU^{(0)}), \qquad E_\theta^{(0)} = \frac{\partial^2 (rU^{(0)})}{r\partial\theta\partial r},$$

$$H_\phi^{(0)} = \frac{ik_\epsilon}{Z_0} \frac{\partial U^{(0)}}{\partial\theta} \qquad (1)$$

where $k_\epsilon = k\sqrt{\epsilon}$, and $Z_0 = (\mu_0/\epsilon_0)^{1/2}$ is the free-space impedance. The so-called electric Debye potential $U^{(0)}$ is ϕ-independent, and is given by

$$U^{(0)}(r, \theta) = \frac{p}{4\pi a} \frac{e^{ik_\epsilon|\mathbf{r} - \mathbf{r}_a|}}{|\mathbf{r} - \mathbf{r}_a|}, \qquad \mathbf{r} = (r, \theta, 0), \quad \mathbf{r}_a = (a, 0, 0)$$

$$(2)$$

where $p = Il$ is the dipole's moment. All of the other field components are zero. Function (2) is connected to the Hertz electric vector potential as $\mathbf{\Pi}_e^{(0)} = U^{(0)}\mathbf{z}_0$.

Due to the rotational symmetry of the scatterer (a disk on top of a layered sphere) and the axial location of RED, the total electromagnetic field vectors $\mathbf{E}$ and $\mathbf{H}$ will have only the same nonzero components as (1): E_r, E_θ, H_ϕ. Denote the substrate as region "(1)," and the outer space as region "(2)." To comply with the solution uniqueness, the total field components must satisfy the following requirements:

1. time-harmonic Maxwell's equations with the wavenumber k or k_ϵ off the conductors and media boundary
2. the set of the boundary and continuity conditions on the complete spherical surfaces:

$$E_\theta^{(1)}(a, \theta) = 0, \qquad 0 < \theta \le \pi \qquad (3)$$

$$E_\theta^{(1)}(c, \theta) = E_\theta^{(2)}(c, \theta) \qquad (4)$$

3. the set of dual conditions on the complementary segments of the spherical surface $r = c$:

$$E_\theta^{(1, 2)}(c, \theta) = 0, \qquad 0 \le \theta < \theta_0 \qquad (5)$$

$$H_\phi^{(1)}(c, \theta) = H_\phi^{(2)}(c, \theta), \qquad \theta_0 < \theta \le \pi \qquad (6)$$

4. the Silber–Muller radiation condition at $r \to \infty$ that can be written as an asymptotic request to the field to behave as an outgoing electromagnetic spherical wave:

$$E_\theta^{(2)} = Z_0 H_\phi^{(2)} = \frac{Z_0 p}{4\pi a} \frac{e^{ikr}}{r} f(\theta) + O\left(\frac{1}{r^2}\right),$$

$$E_r^{(2)} = O\left(\frac{1}{r^2}\right) \qquad (7)$$

where $f(\theta)$ is the far-field radiation pattern
5. the power boundedness condition in any bounded space domain V including the one enclosing the disk rim:

$$\int_V [\epsilon|\mathbf{E}|^2 + |\mathbf{H}|^2] \, dV < \infty. \qquad (8)$$

The last condition determines the edge behavior of the field components: $(E_r, E_\theta = O[(\theta - \theta_0)^{-1/2}], H_\phi = [(\theta - \theta_0)^{1/2}]$, and hence the functional class of the solution sought.

3. DERIVATION OF THE DUAL-SERIES EQUATIONS
The total field in the problem (3)–(8) is naturally decomposed as follows:

$$\mathbf{E}, \mathbf{H} = \begin{cases} \mathbf{E}^{(0)}, \mathbf{H}^{(0)} + \mathbf{E}^{(1)}, \mathbf{H}^{(1)}, & a < r < c \\ \mathbf{E}^{(2)}, \mathbf{H}^{(2)}, & r > c. \end{cases} \qquad (9)$$

To obtain the unknown fields $\mathbf{E}^{(1, 2)}$, $\mathbf{H}^{(1, 2)}$, an electric-field integral equation (EFIE) can be deduced from the boundary condition (5)—see [1, 2]. The other conditions, namely (4) and (6), and the radiation condition (7) can be satisfied due to a proper choice of the kernel functions based on the Green's functions of the layered spherical medium. Due to the singularities in the Green's functions, EFIE is always a hypersingular integral equation. For a numerical solution, EFIE is commonly discretized by using the local-domain or entire-domain expansion functions, the latter frequently taken as so-called cavity-mode functions [2, 11]. However, any of these discretizations fails to guarantee the convergence, in the sense of opportunity to minimize the computational error. This is because conventional moment-method approximations end up with first-kind infinite-matrix equations. In contrast to this, we will work on obtaining a Fredholm second-kind infinite-matrix equation that implies analytical inversion of the singular part of the EFIE. In so doing, one can avoid the EFIE altogether, discretizing the original boundary-value problem from the beginning and working with the series instead of integral equations.

Indeed, the dipole field Debye potential (2) can be expanded, in the substrate, as

$$U^{(0)}(r, \theta) = \frac{ip}{4\pi k_\epsilon ar} \sum_{n=0}^{\infty} (2n + 1)\zeta_n(k_\epsilon r)\psi_n(k_\epsilon a)P_n(\cos\theta)$$

$$(10)$$

where ψ_n and ζ_n are the spherical Bessel and first-kind Hankel functions, respectively, in Debye's notation, and P_n are the Legendre polynomials.

Hence, we will use the latter as the set of entire $(0, \pi)$-domain expansion functions, and seek the secondary field Debye potential in the following form:

$$U^{(1)}(r, \theta) = \frac{ip}{4\pi k_\epsilon ar} \sum_{n=0}^{\infty} (2n+1)[\psi_n(k_\epsilon r)x_n$$
$$+ \zeta_n(k_\epsilon r)y_n]P_n(\cos\theta) \quad (11)$$

$$U^{(2)}(r, \theta) = \frac{ip}{4\pi kar} \sum_{n=0}^{\infty} (2n+1)\zeta_n(kr)z_n P_n(\cos\theta) \quad (12)$$

where x_n, y_n, and z_n are the unknown expansion coefficients to be determined. Electromagnetic field components are then found similarly to (1).

By using conditions (3) and (4), we obtain the relationships between the expansion coefficients of $U^{(1)}$ and $U^{(2)}$:

$$\zeta_n(k_\epsilon a)\psi'_n(k_\epsilon a) + \psi'_n(k_\epsilon a)x_n + \zeta'_n(k_\epsilon a)y_n = 0 \quad (13)$$

$$\psi_n(k_\epsilon a)\zeta'_n(k_\epsilon c) + \psi'_n(k_\epsilon c)x_n + \zeta'_n(k_\epsilon c)y_n$$
$$= \epsilon^{-1/2}\zeta'_n(kc)z_n. \quad (14)$$

These equations enable us to exclude the sets x_n and y_n from further consideration, so that only z_n remain. The dual-boundary conditions (5) and (6) then result in the dual-series equations (DSEs):

$$\sum_{n=1}^{\infty} (2n+1)z_n\zeta'_n(kc)P_n^1(\cos\theta) = 0, \qquad 0 \le \theta < \theta_0 \quad (15)$$

$$\sum_{n=1}^{\infty} (2n+1)z_n\{\zeta_n(kc) + W_n^{-1}\zeta'_n(kc)$$
$$\cdot[\psi_n(k_\epsilon c)\zeta'_n(k_\epsilon a) - \zeta_n(k_\epsilon c)\psi'_n(k_\epsilon a)]\}P_n^1(\cos\theta)$$
$$= \epsilon^{1/2}\sum_{n=1}^{\infty} (2n+1)F_n(kc, a/c, \epsilon)P_n^1(\cos\theta),$$
$$\theta_0 < \theta \le \pi \quad (16)$$

where $P_n^1(\cos\theta)$ are the Legendre functions:

$$W_n = \zeta_n(kc) + \zeta'_n(kc)\frac{\psi_n(k_\epsilon c)\zeta'_n(k_\epsilon a) - \zeta_n(k_\epsilon c)\psi'_n(k_\epsilon a)}{\psi'_n(k_\epsilon a)\zeta'_n(k_\epsilon c) - \psi'_n(k_\epsilon c)\zeta'_n(k_\epsilon a)}$$
$$(17)$$

$$F_n = \psi_n(k_\epsilon a)\zeta_n(k_\epsilon c)$$
$$+ \frac{i\zeta'_n(k_\epsilon c)\psi_n(k_\epsilon c) - \zeta_n(k_\epsilon c)\psi'n(k_\epsilon a)[\psi_n(k_\epsilon a)\zeta'_n(k_\epsilon c) - \zeta_n(k_\epsilon a)\psi'_n(k_\epsilon c)]}{\psi'_n(k_\epsilon a)\zeta'_n(k_\epsilon c) - \psi'_n(k_\epsilon c)\zeta'_n(k_\epsilon a)}. \quad (18)$$

On introducing new unknowns $\tilde{x}_n$,

$$\tilde{x}_n = z_n n(n+1)V_n(kc, c/a, \epsilon) \quad (19)$$

$$V_n = \zeta_n(kc)$$
$$+ W_n^{-1}\zeta'_n(kc)[\psi_n(k_\epsilon c)\zeta'_n(k_\epsilon a) - \zeta_n(k_\epsilon c)\psi'_n(k_\epsilon a)], \quad (20)$$

we can write DSEs in the following form, convenient for further derivations:

$$\sum_{n=1}^{\infty} \frac{2n+1}{n(n+1)}\tilde{x}_n\frac{\zeta'_n(kc)}{V_n}P_n^1(\cos\theta) = 0, \qquad 0 \le \theta < \theta_0 \quad (21)$$

$$\sum_{n=1}^{\infty} \frac{2n+1}{n(n+1)}\tilde{x}_n P_n^1(\cos\theta) = \epsilon^{1/2}\sum_{n=1}^{\infty} (2n+1)F_n P_n^1(\cos\theta),$$
$$\theta_0 < \theta \le \pi. \quad (22)$$

It can be verified that $\tilde{x}_n$ are the expansion coefficients of the surface current on the spherical disk.

4. ANALYTICAL REGULARIZATION

DSEs (21) and (22) can be written compactly in operator notation as $L\tilde{x} = F$. The concept of the method of analytical regularization is based on the inversion of the singular part L_0, so that the rest operator $L - L_0$ is a smooth one [9]. Hence, its product with a bounded inverse to L_0 is a compact operator, which can be approximated by a discrete one with desired accuracy. In the microstrip antenna analysis, we will do this by inverting the static part of a limit form of the DSEs

corresponding to a spherical disk in free space. For this purpose, we verify that $\zeta'_n(kc)V_n^{-1} \to -(2n/(kc(1 + \sqrt{\epsilon})))$ as $n \to \infty$, and introduce the coefficients

$$\gamma_n = 1 + \frac{1 + \sqrt{\epsilon}}{2}kc\frac{2n+1}{n(n+1)}\frac{\zeta'_n(kc)}{V_n}. \quad (23)$$

On so doing, we arrive at DSEs as

$$\sum_{n=1}^{\infty} \tilde{x}_n P_n^1(\cos\theta) = \sum_{n=1}^{\infty} \gamma_n\tilde{x}_n P_n^1(\cos\theta), \qquad 0 \le \theta < \theta_0 \quad (24)$$

$$\sum_{n=1}^{\infty} \frac{2n+1}{n(n+1)}\tilde{x}_n P_n^1(\cos\theta)$$
$$= \epsilon^{1/2}\sum_{n=1}^{\infty} (2n+1)F_n P_n^1(\cos\theta), \qquad \theta_0 < \theta \le \pi. \quad (25)$$

Here, note that $\gamma_n = O(k^2c^2n^{-2}) + O(a^n/c^n)$ as $n \to \infty$. This proves that the operator defined by the left-hand parts of (24) and (25) corresponds to the free-space spherical disk in the static field. Further, we first integrate (24) once, and then use the Mehler−Dirichlet integral representations for the Legendre functions. On changing the orders of summation and integration, we reduce each equation of the DSEs to an Abel integral equation that has a known solution (for details, see [4−8]). This technique exploits the edge behavior of the field function, and brings us to an equivalent series equation in trigonometric functions instead of the Legendre

ones:

$$\sum_{n=1}^{\infty} \tilde{x}_n \cos(n + 1/2)\theta$$

$$= \begin{cases} A\cos(\theta/2) + \sum_{n=1}^{\infty} \gamma_n \tilde{x}_n \cos(n + 1/2)\theta, \\ \quad 0 \le \theta < \theta_0 \\ \epsilon^{1/2} \sum_{n=1}^{\infty} n(n + 1)F_n \cos(n + 1/2)\theta, \\ \quad \theta_0 < \theta \le \pi. \end{cases} \quad (26)$$

The orthogonality and completeness of cosine functions in the interval $(0, \pi)$ enable one to invert the left-hand part of (26). On performing certain algebra in order to exclude the auxiliary constant A, we arrive at the final infinite-matrix equation as follows:

$$\tilde{x}_m - \sum_{n=1}^{\infty} \tilde{x}_n \gamma_n S_{mn} = \epsilon^{1/2} \sum_{n=1}^{\infty} n(n + 1)F_n(\delta_{mn} - S_{mn}),$$
$$m = 1, 2, \ldots \quad (27)$$

where δ_{mn} is Kronecker's delta, and

$$S_{mn}(\theta_0) = \frac{\sin(n - m)\theta_0}{\pi(n - m)} + \frac{\sin(n + m + 1)\theta_0}{\pi(n + m + 1)}$$
$$- \frac{1}{\pi(\theta_0 + \sin\theta_0)}\left(\frac{\sin m\theta_0}{m} + \frac{\sin(m + 1)\theta_0}{m + 1}\right)$$
$$\times \left(\frac{\sin n\theta_0}{n} + \frac{\sin(n + 1)\theta_0}{n + 1}\right). \quad (28)$$

It can be verified that $\sum_{m,n=1}^{\infty} |\gamma_n S_{mn}|^2 < \infty$. Hence, the matrix equation (27) is of the Fredholm second kind in the space of the square-summable number sequences l_2. Therefore, its exact solution exists in this space [12], and can be approximated as accurately as desired by solving progressively larger truncated counterparts of (27). It also can be verified that the field components built after $\tilde{x}_n$ display the needed edge behavior (see [4−6]). Note that filling the matrix in (27) does not require any numerical integrations, unlike in [1, 2]. Very efficient and accurate recurrence codes for computing the Bessel and Hankel functions are readily available, so the entire algorithm happens to be very fast and inexpensive in terms of computer resources. In principle, the accuracy of solving (27) is limited only by the digital precision of the computer.

5. RADIATION CHARACTERISTICS

After determining the coefficients z_n from (27) and (19), one easily can find the surface currents, field components, and overall characteristics of the antenna. First of all, the ϕ-independent far-field radiation pattern [see (7)] is found as

$$f(\theta) = \sum_{n=1}^{\infty} (-i)^n (2n + 1)z_n P_n^1(\cos\theta). \quad (29)$$

Based on this series representation, the total power radiated by the antenna is obtained by integrating the total-field

Poynting vector flux in the far zone:

$$P_{\text{rad}} = \frac{Z_0 p^2}{8\pi a^2} \sum_{n=1}^{\infty} n(n + 1)(2n + 1)|z_n|^2. \quad (30)$$

This power should be compared with the power radiated by a dipole in free space [11]:

$$P_0 = \frac{Z_0 p^2 k^2}{12\pi}. \quad (31)$$

Note that the quantity P_{rad}/P_0 gives the value of the normalized input resistance (radiation resistance) of the microstrip antenna.

It is interesting to calculate the directivity of the antenna as a function of the polar angle θ:

$$D(\theta) = \frac{Z_0 p^2}{4\pi a^2 P_{\text{rad}}}\left|\sum_{n=1}^{\infty} (-i)^n (2n + 1)z_n P_n^1(\cos\theta)\right|^2. \quad (32)$$

To obtain the value of the maximum directivity, one should first determine the angle $\theta_{\max}$ of the main lobe of the radiation pattern, and then calculate $D_{\max} = D(\theta_{\max})$.

6. NUMERICAL RESULTS

Here, we present sample plots characterizing the far-zone radiation of the analyzed antenna. To verify our algorithm, first we have computed the dependence of the computational error, in the "maximum norm" sense:

$$e(N) = \max_{n \le N} |\tilde{x}_n^{N+1} - \tilde{x}_n^N| / \max_{n \le N} |\tilde{x}_n^N| \quad (33)$$

as a function of the matrix (27) truncation number N. It is presented in Figure 2 for three values of the normalized frequency. One can see clearly that a rapid decrement of the error starts near the value of N approximately corresponding to the effective electrical circumference of the substrate $k_\epsilon c$. The Fredholm nature of the matrix guarantees that $e(N) \to 0$ if $N \to \infty$. For practical three-digit accuracy in computing the coefficients $\tilde{x}_n$, the number of equations is to be taken as $N \ge k_\epsilon c + c/h + 10$. What is important in our analysis of a microstrip antenna is the fact that this accuracy is kept uniform, even in the sharp resonances.

In order to find the resonant frequencies of the antenna, we computed the normalized radiated power as a function of the normalized frequency (Fig. 3). The higher the frequency, the lower the amplitudes and Q-factors of the resonances. The latter correspond, in the order of frequency increment, to TM_{01}, TM_{02}, TM_{03}, etc. modes of the "cavity" formed by the patch and the metal sphere. This is confirmed by the far-field radiation patterns computed in the resonances (Fig. 4) that display the appearance of a new sidelobe in the forward half-space for each consecutive resonance. At the same time, it is visible that, if the frequency is high enough, the radiation pattern may have the most intensive beam in the backward half-space, formed by the spherical substrate itself. This is confirmed by a comparative computation of the direction of the main-beam radiation, and the directivities in the main-beam direction, for a dipole-fed microstrip antenna and for a dipole in the spherical substrate covering a PEC sphere (without the disk). These plots are presented in Figures 5 and 6, respectively. Figure 5, in particular, demonstrates the above-mentioned "keel over" of the main-beam
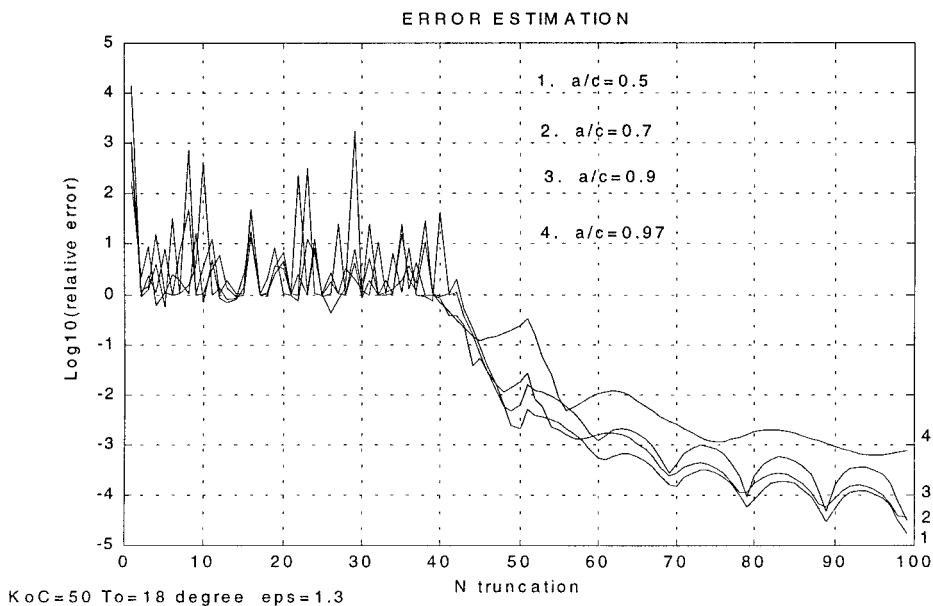
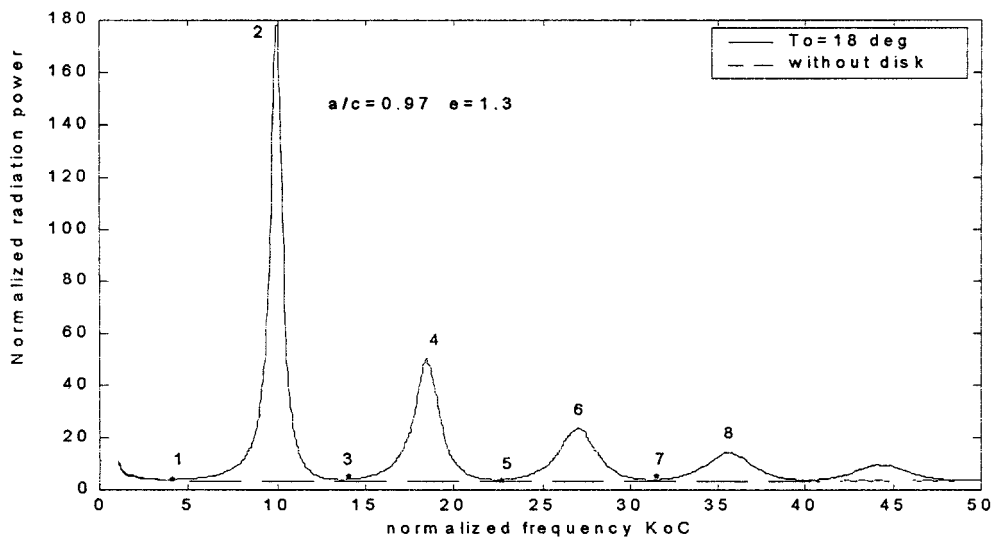**Figure 2** Relative computational error as a function of the matrix truncation number

Figure 3 Normalized radiation resistance (normalized radiated power) as a function of the normalized frequency. Antenna parameters are: $\theta_0 = 18°$, $\epsilon = 1.3$, $a/c = 0.97$. Figure marks correspond to the patterns in Figure 4

radiation direction, both for a conformal microstrip antenna and for a dipole, if the frequency becomes higher. The presence of the patch, however, shifts the "keel-over" frequency to a much greater value. The appearance of strong radiation in the backward sector can be attributed to the interference of the creeping waves circumnavigating around the spherical substrate.

7. CONCLUSIONS

We have presented an accurate modeling method and numerical results related to a spherical–circular microstrip antenna, under an axially symmetric excitation by an electric dipole. Due to analytical inversion of the singular part of the prob-

lem, the resulting algorithm is very efficient. Accuracy is controllable and uniform, even in the resonances. Numerical study hence delivers reliable information on the antenna performance. Such a study confirms intuitive considerations that a patch plays the role of a resonant amplifier of the radiation resistance of the dipole that is otherwise understandably small. We have found that, as the frequency of operation increases, the patch fails to provide a favorable radiation pattern, and the latter is formed mainly by the spherical substrate. Thus, generally speaking, the radiation of this conformal antenna is principally different from the same on an infinite flat-layered substrate, although in the frontal sector, the two can be close to each other.
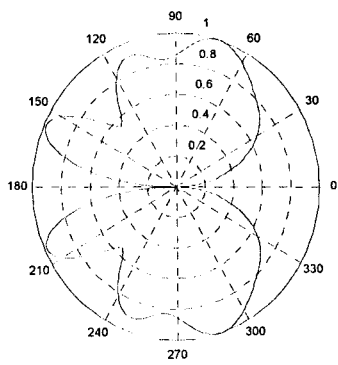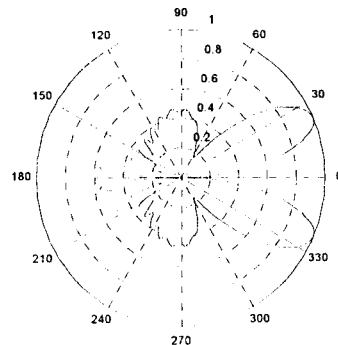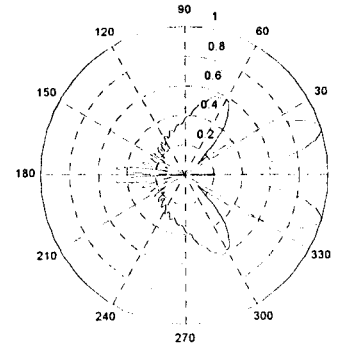
1

KoC=4 a/c=0.97 To=18 e=1.3
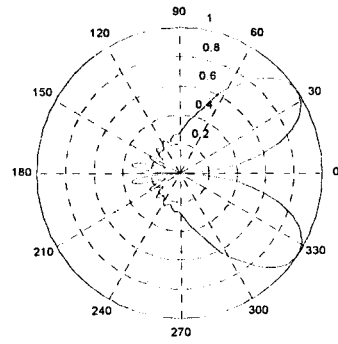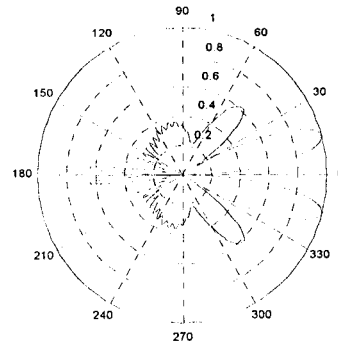
2

KoC=9.9743 a/c=0.97 To=18 e=1.3
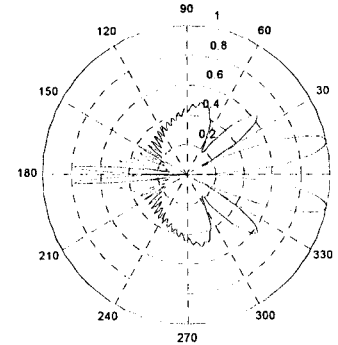
3

KoC=14 a/c=0.97 To=18 e=1.3
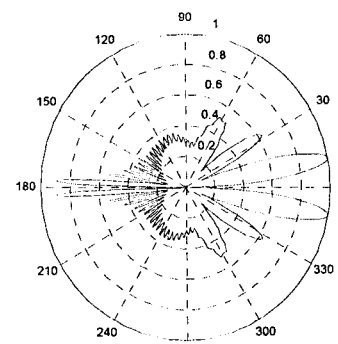
4

KoC=18.495 a/c=0.97 To=18 e=1.3

5

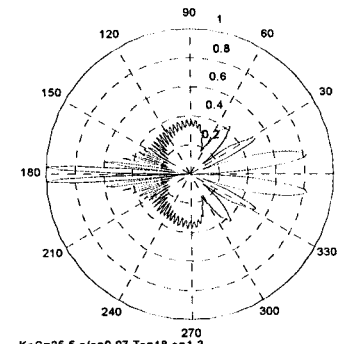KoC=22.5 a/c=0.97 To=18 e=1.3

6

KoC=26.9 a/c=0.97 To=18 e=1.3

7

KoC=31.2 a/c=0.97 To=18 e=1.3

8

KoC=35.5 a/c=0.97 To=18 e=1.3

Figure 4 Normalized far-field patterns at the frequencies marked in Figure 3
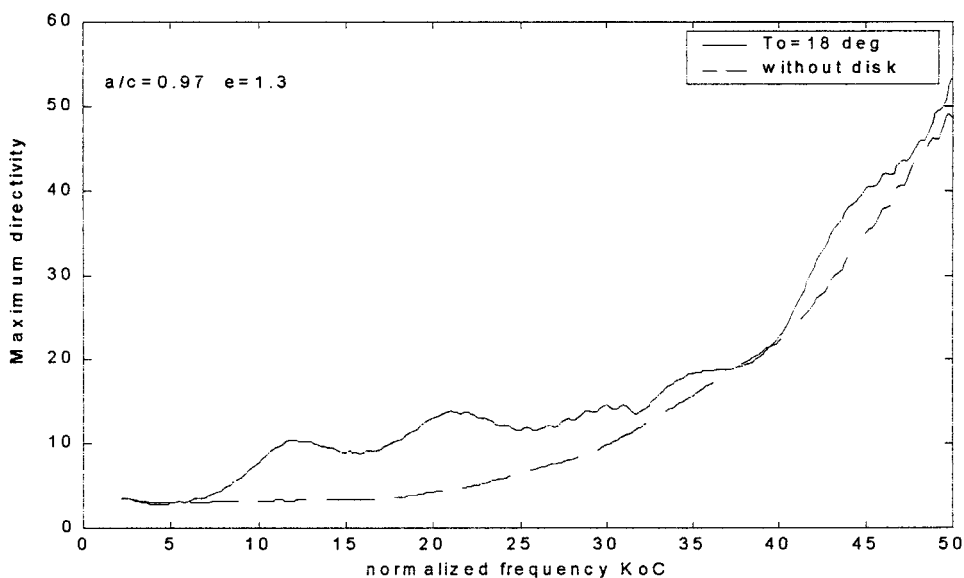
Figure 5 Directivity in the main-beam direction as a function of the normalized frequency. The antenna parameters are the same as in Figure 3
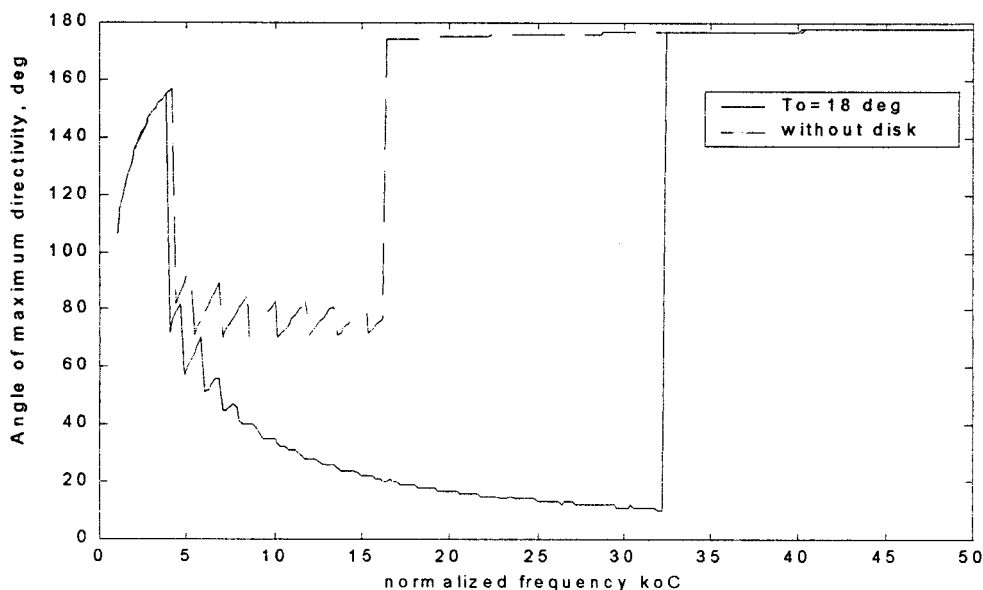

Figure 6 Main-beam radiation angle as a function of the normalized frequency. The antenna parameters are the same as in Figures 3 and 5

REFERENCES

1. B. Ke and A.A. Kishk, Analysis of spherical circular microstrip antennas, Proc Inst Elect Eng 138 (1991), 542–548.

2. K.-L. Wong, S.-F. Hsiao, and H.-T. Chen, Resonance and radiation of a superstrate-loaded spherical-circular microstrip patch antenna, IEEE Trans Antennas Propagat 41 (1993), 686–690.

3. G.L. Hower, R.G. Olsen, J.D. Earls, and J.B. Schneider, Inaccuracies in numerical calculation of scattering near natural frequencies of penetrable objects, IEEE Trans Antennas Propagat 41 (1993), 982–986.

4. S.S. Vinogradov, A soft spherical cap in the field of a plane sound wave, USSR J Comput Maths Math Phys (English transl.) 18 (1978), 244–249.

5. S.S. Vinogradov, Y.A. Tuchkin, and V.P. Shestopalov, Summatory equations with kernels in the form of Jacobi polynomials, Sov Phys Dokl (English transl.) 25 (1980), 531–532.

6. S.S. Vinogradov, Reflectivity of a spherical shield, Radiophys Quantum Electron (English transl.) 26 (1983), 78–88.

7. R.W. Ziolkowski, D.P. Marsland, L.F. Libelo, and G.E. Pisane, Scattering from an open spherical shell having a circular aperture and enclosing a concentric dielectric sphere, IEEE Trans Antennas Propagat 36 (1988), 985–999.

8. S.S. Vinogradov, E.D. Vinogradova, A.I. Nosich, and A. Altintaş, Analytical regularization based analysis of a spherical reflector symmetrically illuminated by an acoustic beam, J Acoust Soc Amer 107 (2000).

9. A.I. Nosich, The method of analytical regularization in wave-scattering and eigenvalue problems: Foundations and review of solutions, IEEE Antennas Propagat Mag 43 (1999), 34–49.

10. J.J. Bowman, T.B.A. Senior, and P.L.E. Uslenghi, Electromagnetic and acoustic scattering by simple shapes, Hemisphere, New York, 1987.

11. W.L. Stutzman and G.A. Thiele, Antenna theory and design, Wiley, New York, 1998.

12. D.S. Jones, Methods in electromagnetic wave propagation, Clarendon, Oxford, England, 1994.